Journal of the European Ceramic Society **14** (1994) 189–204

Synthesis of Monodispersed Silica Powders I. Particle Properties and Reaction Kinetics

Herbert Giesche

New York State College of Ceramics at Alfred University, School of Ceramic Engineering and Science, 2 Pine Street, Alfred, New York 14802-1296, USA

(Received 6 December 1993; revised version received 23 February 1994; accepted 8 March 1994)

Abstract

Currently there are several models discussed to describe the formation of monodispersed silica particles by the controlled hydrolysis and condensation of tetraethylorthosilicate (TEOS) in mixtures of water/ammonia and ethanol. The present study will show results on an extended range of experimental conditions.

Particle growth followed a first-order reaction kinetic with respect to TEOS concentration. Reaction orders for the ammonia and water content were 0·97 and 1·18, respectively. Only monomeric (≈ 70–90%) and dimeric (≈ 10–25%) silicate units were detected during the growth reaction and an activation energy of 27 kJ mol^{-1} (6·5 kcal mol^{-1}) was indicated. Particles revealed an ultramicroporous internal structure. A narrower size distribution and a more spherical shape were observed at higher water concentrations.

The results suggested an aggregation mechanism of nanometer-sized primary nuclei during the first stage of the reaction followed by a monomer addition growth mechanism thereafter.

Zur Zeit werden verschiedene Modelle untersucht, welche die Bildung monodisperser SiO_2-Teilchen durch Hydrolyse und Kondensation von TEOS in Wasser/Ammoniak und Ethanol Gemischen beschreiben. Die vorliegende Arbeit zeigt Ergebnisse in einem erweiterten experimentellen Bereich.

Das Partikelwachstum verlief entsprechend einer Reaktion erster Ordnung bezüglich der TEOS Konzentration. Die Reaktionsordnung bezüglich der Ammoniak- und Wasser-Konzentration war 0·97 bzw. 1·18. Während der Reaktion wurden vornehmlich monomere (≈ 70–90%) und dimere (≈ 10–25%) Kieselsäure-Einheiten beobachtet. Die Aktivierungsenergie betrug 27 kJ mol^{-1} (6·5 kcal mol^{-1}). Die Partikel zeigten ein ultramikroporöse Struktur. Bei höheren Wassergehalten war die Teilchengrößenverteilung enger und die Form sphärischer.

Die Ergebnisse legen einen Wechsel im Reaktionsmechanismus nahe. Zu Beginn lagern sich nanometer große Primärpartikel zu Agglomeraten zusammen und ab einem bestimmten Zeitpunkt erfolgt das Partikelwachstum durch Kondensation monomerer Kieselsäureeinheiten an der Partikeloberfläche.

Il existe actuellement plusieurs modèles permettant de décrire la formation de particules monodispersées de silice par hydrolyse et condensation contrôlées du tetraéthylorthosilicate (TEOS) dans des mélanges eau/NH_3 et éthanol. L'étude présentée montre des résultats obtenus pour une gamme très large de conditions expérimentales. La croissance des particules est liée à la cinétique d'une réaction du premier ordre, elle-même dépendante de la concentration en TEOS. Les ordres réactionnels pour des solutions contenant de l'eau et de l'ammoniac sont respectivement de 0·97 et 1·18. Seuls des monomères (70–90%) et des dimères (10–25%) de silicates se forment, et l'énergie d'activation est de 27kJ mol^{-1}. (6·5 kcal mol^{-1}). Les particules présentent une structure interne ultra-microporeuse. On peut également observer une distribution plus serrée et une sphéricité plus marquée des particules, lorsque la concentration en eau augmente. L'interprétation des résultats est la suivante: présence d'un mécanisme d'agrégation de noyaux primaires de taille nanométrique (durant la première partie de la réaction) suivi d'un mécanisme de croissance additionnelle de monomères.

1 Introduction

Already in 1956 Gerhard Kolbe[1] observed the formation of spherical silica particles, when tetraethylorthosilicate was hydrolysed in the

Journal of the European Ceramic Society 0955-2219/94/$7.00

presence of ammonia. In 1968 Stöber *et al.*[2] took up and improved this process to produce exceptional monodispersed silica particles. The final particle size could be controlled reasonably well within a wide range, and particles of up to 1·5 μm were prepared. Irrespective of this result it was just a few years ago that a renaissance of this process took place, when a number of scientists started to use these powders as model systems in various areas; e.g. light-scattering studies,[3-6] the rheology of dispersions,[7-11] formation of ordered sediments,[11-14] or the sintering of model powder compacts.[13-16] Despite the increased number of applications of these 'Stöber' silica powders, the reaction pathway still remained vague, due to the relative fast reaction rate and various reaction intermediates, until very recently the nucleation and growth process was studied in more detail.[13,17-28] At present the process is not resolved completely, but all interpretations of the experimental results focus on two models: a monomer-addition and a nucleation–aggregation growth model. A combination of both models will probably best describe the entire process. Switching from a nucleation–aggregation mode to a monomer-addition process as the reaction proceeds and depending on the overall starting conditions.

The first part of the present paper will reveal a series of well-defined experiments describing the silica precipitation process. The influences of the starting reaction conditions on particle properties (size, size distribution and shape) and reaction kinetics (reaction rate and induction period) were studied over a wide range. The results were completed by gas chromatography and gas adsorption experiments as well as a statistical analysis of several reaction parameters. In a second part, a controlled growth procedure will be presented, which allows a given particle size of up to several μm in diameter having an even narrower size distribution to be prepared exactly. Moreover, a continuous production process of such monodispersed silica particles will be described.

2 Experimental

2.1 Particle preparation (one step)

Tetraethylorthosilicate (TEOS; Wacker, Burghausen, Germany) was distilled immediately before use. Prior to the distillation, CaO was added in order to capture HCl impurities, which often remained from the synthesis of TEOS. All other chemicals were used without further purification. Ethanol (E. Merck, Darmstadt, Germany) was denatured with methyl ethyl ketone. Ammonia solution (25%; E. Merck, Darmstadt, Germany) was analytical grade. Some experiments required a higher NH_3 concentration in relation to the permitted water content. In order to achieve this, part of the regular ethanol was replaced by ethanol saturated with ammonia. The latter was prepared by bubbling NH_3 through the ethanol at 195 K (−78°C) until the ammonia concentration reached about 6 mol dm^{-3}. All ammonia concentrations were checked in the final solutions (prior to the precipitation) by titration with HCl. The water and TEOS concentrations were calculated from the weight fractions of the different portions.

The precipitation proceeded as follows. Mixture A—alcohol, water and ammonia—and mixture B—TEOS in alcohol (1 : 1 volume ratio)—were heated in closed containers to the desired temperatures. Then mixture A was put in a round-bottomed flask, equipped with a paddle stirrer and a condenser and placed in a constant temperature bath. Thereafter mixture B was added under vigorous stirring (1000 rpm). The mixing was stopped after 15 s. In spite of the constant temperature bath, the temperature in the centre of the reaction vessel increased slightly by up to 2 K during the first few minutes after the addition of TEOS, which was due to the exothermic character of the reaction.

2.2 Light scattering

The growth of particles in the solution was followed with a very simple light scattering device. An IR-sensitive photoelectric barrier was used for this purpose. The emitter and detector were cut and adjusted to fit into two NMR tubes. Figure 1 shows the schematic drawing of the device. Emitter and detector were positioned at an angle of 90° and an additional shielding prevented any direct optical path between them. The device fitted into the reaction flask and the particle growth reaction could be recorded *in situ*. After a careful calibration with various suspensions having a known particle size and concentration, the actual particle size and concentration during the reaction or the reaction conversion, could be calculated from the detector signal. The light-scattering intensity was approximately proportional to the particle mass over most of the evaluated range. Further details are listed elsewhere.[13]

2.3 Trimethylsilylation

Trimethylsilylation, also called 'end-capping', is a well-established characterization method for low molecular weight silicate units.[29-32] The reaction transforms Si–OH groups into non-polar (hydrophobic) Si–O–Si$(CH_3)_3$ groups. The latter groups are very stable with temperature or towards any further reaction. Due to the hydrophobic charac-

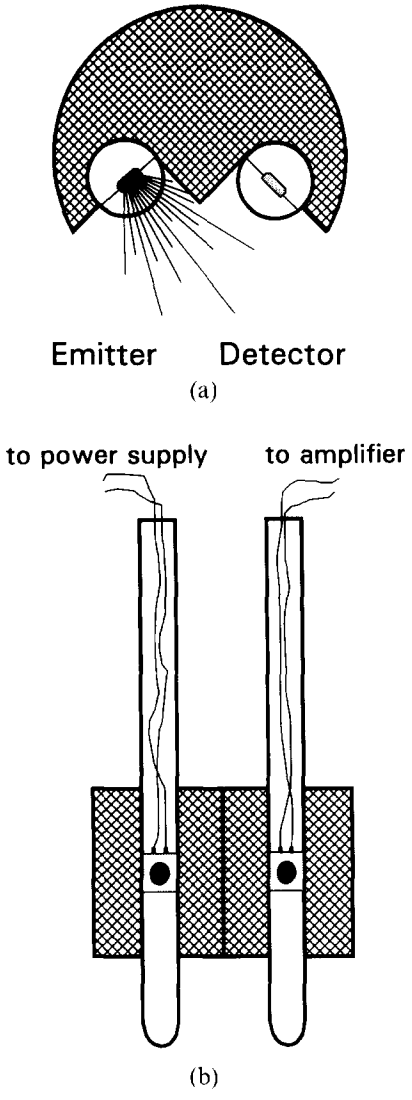

Fig. 1. Sectional drawing, (a) horizontal and (b) vertical, of the light scattering device.

ter of the end-capped reaction products, the latter can be separated by extraction with non-polar solvents. A qualitative and quantitative gas chromatographic analysis followed.

The experiments shown here were performed in an analogous way as described by Bechtold *et al.*[31] After various periods of time from the start of the hydrolysis, samples were taken from the reaction mixture and added under vigorous stirring to the same volume of trimethylchlorosilane. The mixture was cooled in an ice bath, since the reaction had a very exothermic character. Two layers formed and the water-insoluble products were extracted with methylene chloride, washed with water and dried with Na_2SO_4. After filtering off the Na_2SO_4, methylene chloride (solvent) and hexamethyldisiloxane (the self-condensation product of trimethylchlorosilane) were removed by evaporation. The 'frozen' particle sizes could be inspected by TEM in the so-prepared samples and the low molecular weight building units were characterized by gas chromatography (GC).

A gas chromatograph 4300 (Carlo Erba) equipped with a capillary column, OV-1, and a flame ionization detector was used for the GC analysis. The carrier gas was nitrogen at a pressure of 0·077 MPa and the FID (flame ionization detector) gases, hydrogen and oxygen, were adjusted to pressures of 0·05 MPa and 0·10 MPa, respectively. The temperature of the injection block was 573 K (300°C) and that of the detector was 623 K (350°C). The best separation of the different silicate species was achieved by a temperature program starting at 388 K (115°C) and increasing at a heating rate of 10 K min^{-1} up to a final temperature of 573 K(300°C). The retention times and FID response factors were in accordance to results by Garzo *et al.*[30] and Schubert,[32] who worked at the same GC conditions. The latter results could be used to verify and characterize all chromatographic peaks.

2.4 Transmission electron microscopy (TEM)

TEM micrographs were obtained at a Philips (Kassel, Germany) Model EM 300 electron microscope. The acceleration voltage of the electron beam was 80 kV. TEM was employed to determine the particle size and structure of the silica beads. Copper carrier grids were covered with a carbon film. One drop of the properly diluted particle dispersion was put onto these grids and dried. In order to improve the accuracy of the magnification, the TEM was calibrated with a grating replica prior to the measurements.

The size and shape of the observed particles were evaluated from the micrographs with the help of an image analysing system, Kontron Videoplan System (Kontron, Munich, Germany). On a magnetic board the particle profiles were traced with a pen. Particle size and shape was calculated from these computerized data (the projected particle area). The mean particle size was the equivalent of a circle having the same area and the shape factor was the axial ratio of an ellipse, having the same inertial moment as the copied structure. Over 200 particles were measured for each sample and the standard deviation was calculated from the fit of these data to a Gaussian probability distribution. Due to the narrow size distributions of almost all samples, the number of analysed particles per sample was sufficient to guarantee accurate values. However, the measuring method had a certain error in itself, which was checked with the help of a test sample. Circles of exactly 3 cm, 2 cm, and 1·5 cm in diameter were measured 100 times. The absolute value for the standard deviation was about ±0·016 cm for all circle sizes, corresponding to relative errors between ±0·5% and ±1·1%. Therefore all TEM micrographs were enlarged to result in particle

diameters of 2 to 3 cm on the photographs, which reduced the error of the method to less than 1%. Nevertheless, the latter effect has to be taken in mind for some of the samples having a standard deviation of 2% or less.

2.5 Gas adsorption

Nitrogen sorption isotherms were determined at 77 K (−196°C), using a microbalance (model 4102 or 4434; Sartorius, Göttingen, Germany). Prior to the nitrogen adsorption samples were degassed at 473 K (200°C) until the sample mass remained constant (10 h, final vacuum 10^{-4} Pa). Nitrogen was of 99·999% purity (Linde, Düsseldorf, Germany). The saturation vapour pressure of nitrogen was measured close to the sample, employing a specially constructed device[13,33]. The pressure was recorded with a piezo-resistive pressure transducer (Model 4043Al; Kistler, Ostfildern, Germany). The specific surface area was calculated from the nitrogen sorption data according to the BET equation, using a molecular cross-sectional area of 0·162 nm^2 for the nitrogen molecule.

Sorption measurements of helium, argon, krypton and xenon (purity > 99·99%, Messer, Griesheim, Germany) were performed in a similar way on the dried and calcined silica samples at 298 K (25°C), using a magnetic suspension balance (Model 4201; Sartorius, Göttingen, Germany) and a capacitive-resistive membrane pressure transducer (Model Baraton 220B; MKS).

2.6 Apparent helium and water densities

The apparent He density, d_{app}(He), was determined on a helium pycnometer (Model 930; Beckman, Munich, Germany). The total volume of the sample cell was ≈10 cm^3 and the sample volume could be determined with an accuracy of ±0·03 cm^3, corresponding to a relative error of 0·5–1%.

The apparent water density, $d_{app}(H_2O)$, was measured at 298 K (25°C), using a small pycnometer of ≈0·8 cm^3 volume. The reproducibility of these density measurements was about ±0·15%.

3 Results and Discussion

The silica precipitation reaction was studied over the following range of starting conditions: TEOS 0·1–0·4 mol dm^{-3}; NH_3 0·8–4·2 mol dm^{-3}; H_2O 3·0–13·0 mol dm^{-3}, and reaction temperature 293–333 K (20–60°C). Table 1 presents the experimental results in terms of particle properties and reaction kinetics. The systematic set-up of the reaction conditions allows for a statistical analysis of all parameters and various combined effects. The factorial analysis was performed according to the general procedure described by Davies.[34] Further details are described elsewhere.[13] The parameters were analysed in terms of a linear or quadratic effect and the various combined effects of these parameters on the observed characteristic property. Tables 2 and 3 summarize the results of the calculations. As shown earlier, the precipitation reaction was relatively independent of the experimental procedure (e.g. mixing time or stirring speed), provided that the reactants were thoroughly mixed within a reasonable time (less than the induction period, described in further detail later). Nonetheless, the highest degree of reproducibility was assured, when the procedure was performed in a very controlled way, as described in the experimental part. As an example,

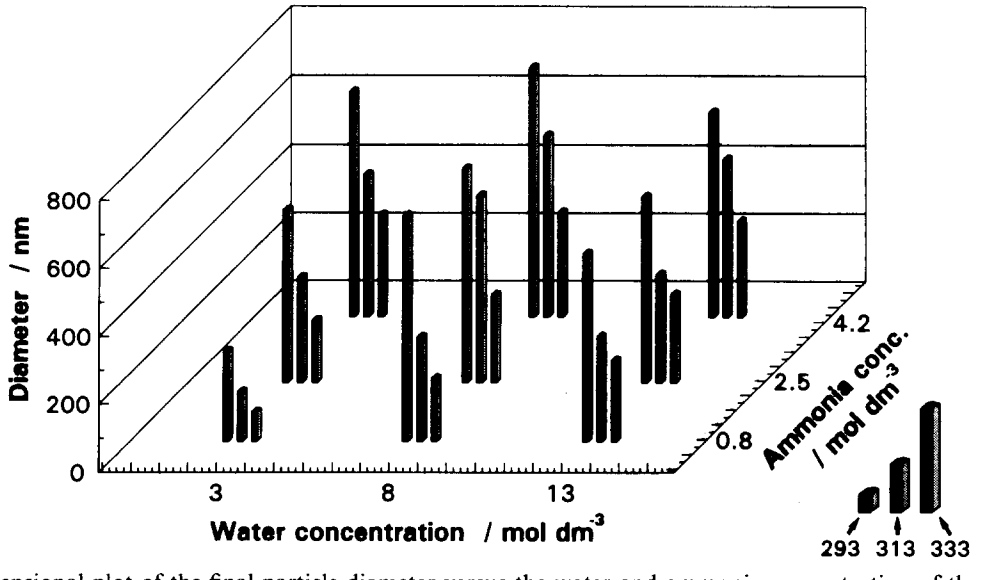

Fig. 2. Three-dimensional plot of the final particle diameter versus the water and ammonia concentration of the reaction mixture at a constant TEOS concentration of 0·2 mol dm^{-3}. The left, middle and right bars of each data triple indicate results at reaction temperatures of 293, 313, 333 K (20, 40, 60°C), respectively.

Table 1. Particle properties (particle diameter, standard deviation of the size distribution and shape factor) and experimental data of the reaction kinetics (first-order reaction rate, k_{TEOS}, and induction time) listed for the various reaction mixtures

Reaction conditions				*Particle properties*			*Reaction kinetics*	
H_2O (mol dm^{-3})	NH_3 (mol dm^{-3})	TEOS (mol dm^{-3})	Temperature (K)	Diameter (nm)	Standard deviation (nm)	Shape factor	k_{TEOS} (10^{-3} s^{-1})	Induction time (10^3 s)
3	0·8	0·1	293	274	14·2	0·959		
3	0·8	0·2	293	267	26·7	0·953	0·166	1·63
3	0·8	0·4	293	161	25·6	0·924		
3	0·8	0·2	313	146	12·6	0·936	0·124	1·15
3	0·8	0·1	333	88·7	10·0	0·902		
3	0·8	0·2	333	87	8·5	0·883	0·85	0·79
3	0·8	0·4	333	86·3	8·3	0·890		
8	0·8	0·2	293	665	25·0	0·950	0·254	0·290
8	0·8	0·2	313	309	15·2	0·960	0·345	0·300
8	0·8	0·2	333	186	10·5	0·963	1·07	0·250
13	0·8	0·1	293	283	31·7	0·922		
13	0·8	0·2	293	555	15·5	0·963	0·61	0·176
13	0·8	0·4	293	692	16·0	0·949		
13	0·8	0·2	313	310	12·4	0·961	1·89	0·121
13	0·8	0·1	333	166	15·3	0·946		
13	0·8	0·2	333	240	12·8	0·960	2·14	0·101
13	0·8	0·4	333	224	9·0	0·965		
3	2·5	0·2	293	510	28·0	0·925	0·65	0·432
3	2·5	0·2	313	311	25·0	0·896	0·479	0·391
3	2·5	0·2	333	185	14·8	0·935	0·97	0·287
8	2·5	0·2	293	633	11·3	0·964	0·71	0·153
8	2·5	0·2	313	550	11·7	0·960	1·66	0·074
8	2·5	0·2	313	572	12·1	0·955	2·38	0·086
8	2·5	0·2	313	537	10·9	0·958	1·75	0·079
8	2·5	0·2	333	260	20·0	0·967	4·20	0·070
13	2·5	0·2	293	550	11·7	0·962	2·25	0·108
13	2·5	0·2	313	320	13·8	0·968	2·99	0·052
13	2·5	0·2	333	261	16·7	0·968	7·40	0·034
3	4·2	0·1	293	588	22·7	0·944		
3	4·2	0·2	293	660	40	0·880	0·373	0·300
3	4·2	0·4	293	660		Agglomerate		
3	4·2	0·2	313	421	25·7	0·929	1·09	0·198
3	4·2	0·1	333	242	10·8	0·960		
3	4·2	0·2	333	300	30·5	0·943	0·92	0·188
3	4·2	0·4	333	395	49·8	0·927		
8	4·2	0·2	293	730	50	0·870	1·11	0·121
8	4·2	0·2	313	534	32·0	0·955	2·29	0·058
8	4·2	0·2	333	310	15·0	0·961	6·3	0·057
13	4·2	0·1	293	417	8·2	0·949		
13	4·2	0·2	293	602	9·8	0·963	2·12	0·078
13	4·2	0·4	293	600		Agglomerate		
13	4·2	0·2	313	466	8·0	0·954	5·9	0·0408
13	4·2	0·1	333	271	9·1	0·962		
13	4·2	0·2	333	283	11·4	0·966	13·4	0·0273
13	4·2	0·4	333	308	8·6	0·967		

one experiment was repeated five times and the resulting mean particle diameter was consistent within ±2·5%.[35]

3.1 Particle size

The statistical analysis (see Tables 2 and 3) indicated the significance of several experimental parameters on the final particle size. The reaction temperature (lin; linear) ammonia concentration (lin), and water concentration (sq; quadratic) clearly influenced the particle size, as shown by the high variance ratios (above a level of significance of 99%). The importance of the water concentration (lin), TEOS concentration (lin) and the combined effect of ammonia (lin)/water (lin) concentrations was suggested with a probability of >95%, whereas effects of water (sq)/temperature (lin) or water/TEOS (lin) were observed at a level of only 90%. All other parameters or combinations seemed to be of minor importance. Irrespective of these conclusions, the statistical analysis can only show that certain parameters influence the particle size, but it can not tell how much or in which direction the size will be influenced. The three-dimensional graph in Fig. 2 can give a much better answer to the last question. With decreasing temperature or increasing ammonia concentration particles became larger, whereas the effect of the

Table 2. Factorial analysis of the experiments shown in Table 1

Reciprocal effect	*Variance ratio*				
	Size	*Standard deviation*	*Shape*	k_{TEOS}	*Induction time*
NH_3(lin)	**42·18**	7·10	2·26	**96·71**	**92·70**
NH_3(sq)	0·05	1·06	1·20	0·24	**15·66**
H_2O(lin)	8·70	10·20	**28·76**	**155·49**	**141·95**
H_2O(sq)	**20·92**	1·12	1·47	2·97	**24·74**
Temperature(lin)	**166·31**	6·21	2·61	**119·57**	**14·59**
Temperature(sq)	1·79	0·71	0·22	6·09	0·21
NH_3(lin)/H_2O(lin)	10·74	5·52	0·11	**51·61**	**68·87**
NH_3(sq)/H_2O(lin)	0·94	0·27	0·16	0·14	11·71
NH_3(lin)/H_2O(sq)	0·79	1·59	2·27	0·28	**12·32**
NH_3(sq)/H_2O(sq)	0·40	2·88	1·58	0·53	1·73
NH_3(lin)/Temperature(lin)	0·41	3·09	**13·70**	**41·79**	5·27
NH_3(sq)/Temperature(lin)	0·08	1·02	0·34	0·32	1·11
NH_3(lin)/Temperature(sq)	1·62	0·08	0·25	1·95	0·02
NH_3(sq)/Temperature(sq)	0·57	0·00	2·70	0·53	0·04
H_2O(lin)/Temperature(lin)	0·09	0·09	0·00	**57·36**	8·00
H_2O(sq)/Temperature(lin)	5·08	3·23	4·08	0·02	0·01
H_2O(lin)/Temperature(sq)	0·02	0·02	0·04	2·35	2·82
H_2O(sq)/Temperature(sq)	0·92	0·28	0·78	0·12	0·01
NH_3(lin)/H_2O(lin)/Temperature(lin)	1·20	0·04	7·04	**31·23**	7·38

The value of the variance ratio indicated the probability of a reciprocal effect on the evaluated parameter. Experimental parameters: TEOS concentration, 0·2 mol dm^{-3}; ammonia concentration, 0·8, 2·5, 4·2 mol dm^{-3}; water concentration, 3·0, 8·0, 13·0 mol dm^{-3}; temperature, 293, 313, 333 K. The abbreviations (lin) and (sq) represent linear and quadratic reciprocal effects.
The different levels of significance are: low (α = 0·90) for a variance ratio >3·59; high (α = 0·95) for a variance ratio >5·59; very high (α = 0·99) for a variance ratio >12.20.

water concentration clearly indicated a maximum of the particle size around a concentration of 8 mol dm^{-3}. The results shown here are in agreement with the original work of Stöber *et al.*[2] and other groups.[21,36,37] However, the results presented here cover a much broader range of conditions (e.g. the influence of the reaction temperature was not studied in such a systematic way by others).

Table 3. Factorial analysis of the experiments shown in Table 1

Reciprocal effect	*Variance ratio*		
	Size	*Standard deviation*	*Shape*
NH_3	**23·76**	6·21	1·14
H_2O	3·39	5·36	5·69
Temperature	**46·12**	**8·61**	3·32
TEOS (lin)	4·66	**7·35**	**7·35**
TEOS (sq)	0·69	0·23	1·55
NH_3/H_2O	**11·93**	**6·98**	0·08
NH_3/Temperature	0·74	0·02	**12·43**
H_2O/Temperature	0·30	0·01	1·45
NH_3/TEOS (lin)	0·06	**11·64**	**7·26**
NH_3/TEOS (sq)	0·03	0·14	0·42
H_2O/TEOS (lin)	2·45	2·60	1·13
H_2O/TEOS (sq)	0·17	1·28	1·27
Temperature/TEOS (lin)	0·69	0·95	5·56
Temperature/TEOS (sq)	0·51	0·43	1·93

The value of the variance ratio indicated the probability of a reciprocal effect on the evaluated parameter. Experimental parameters: TEOS concentration, 0·1, 0·2, 0·4 mol dm^{-3}; ammonia concentration, 0·8, 4·2 mol dm^{-3}; water concentration, 3·0, 13·0 mol dm^{-3}; temperature, 293, 333 K. (lin), Linear; (sq), quadratic.
The different levels of significance are: low (α = 0·90) for a variance ratio >2·73; high (α = 0·95) for a variance ratio >3·74; very high (α = 0·99) for a variance ratio >**6.71**.

3.2 Particle size distribution

In a similar way the influence of the reaction conditions on the width of the particle size distribution (standard deviation) was analysed. The latter was controlled by the same parameters, but their effect was less pronounced, as shown by the lower values of the variance ratios (see Table 2). Figure 3 illustrates the tendency towards a narrower size distribution at higher water concentrations. However, Fig. 3 does not allow the influence of other parameters like the temperature, the ammonia or TEOS concentrations to be interpreted; even so, statistics indicated their effect on a confidence level of > 99 or 95% (see Tables 2 and 3). A lower limit of about ±10 nm was observed for the absolute value of the standard deviation, irrespective of the mean particle size of the samples (valid only for the samples shown here!). Yet it has to be mentioned that the size distributions could be smaller than ±10 nm, when the mean particle size fell below 100 nm at even lower ammonia or water concentrations, or when a controlled growth process was applied,[13,38] as described in part two of this study.

3.3 Particle shape

The 'shape factor' of the silica particles was evaluated from the TEM micrographs as described in the experimental part. TEM pictures could give only a two-dimensional view of the particles and it is probable that the actual shape was somewhat different from the two-dimensional value. How-

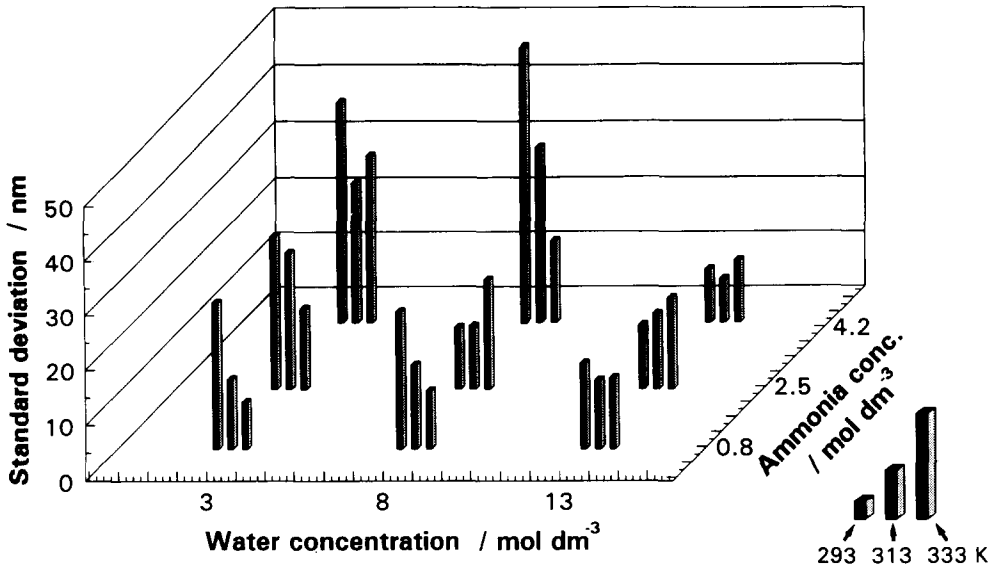

Fig. 3. Three dimensional plot of the standard deviation (number distribution of the particle diameter) versus the water and ammonia concentration of the reaction mixture at a constant TEOS concentration of 0·2 mol dm^{-3}. The left, middle, and right bars of each data triple indicate results at reaction temperatures of 293, 313, 333 K (20, 40, 60°C), respectively.

ever, in contrast to needles or platelets, there was no preferred particle orientation to worry about, when these particles were lying on a flat surface. Due to the (relatively) spherical shape of nearly all particles, only minor differences between the measured and actual shape were expected.

The particle shape could deteriorate from that of a perfect sphere due to agglomeration processes or inhomogeneous conditions during the growth period of the particles. As indicated in the factorial analysis, the water concentration (lin), TEOS concentration (lin) and the combined effect of ammonia (lin)/temperature (lin) or ammonia/TEOS concentration (lin) had a highly significant influence (>99%) on the shape. Furthermore the three parameter interaction of water (lin)/ammonia (lin)/temperature or temperature/TEOS concentration (lin) were also significant at a level of >95%. Figure 4 presents the results in a similar three-dimensional graph as was shown before for the mean particle size values of the samples. It was obvious from this diagram that the produced particles tended to be more spherical at higher water concentrations. Nonetheless, the results have to be interpreted with great caution, since the shape was closely related to and 'influenced by' the mean particle size. In general, small particles (<100 nm ∅ (diameter)) tended to be not as spherical as particles of larger sizes. The explanation was very simple, inasmuch as inhomogeneities appearing during the early stages of the particle precipitation can be equalized during the latter growth process. On the other hand, conditions which produced larger sizes (>600 nm ∅) were often accompanied

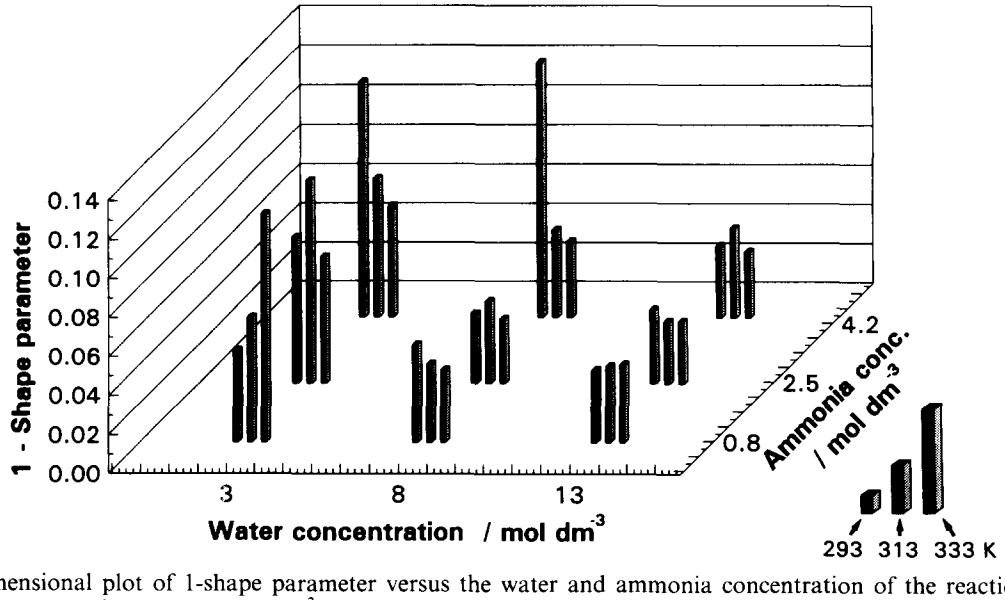

Fig. 4. Three-dimensional plot of 1-shape parameter versus the water and ammonia concentration of the reaction mixture at a constant TEOS concentration of 0·2 mol dm^{-3}. The left, middle and right bars of each data triplet indicate results at reaction temperatures of 293, 313, 333 K (20, 40, 60°C), respectively.

by agglomeration and the latter process, likewise, deteriorated the particle shape.

3.4 Particle structure

The silica powders were X-ray amorphous, even after a calcination at 1373 K (1100°C) for several days. Only at calcination temperatures above 1573 K (1300°C) was α-cristobalite formed.

DTA and TG analysis indicated the loss of adsorbed water (≈ 5 wt %) below 473 K (200°C) and an increasing dehydroxylation process (≈ 5 wt %) at higher temperatures (up to 1073 K (800°C)).

Moreover, considerable amounts of ammonia were strongly bound to or incorporated in the silica particles. For example, a significant shift of the pH of an aqueous dispersion was noticed with time. This process was caused by the release of ammonia from the silica particles. Several washing cycles or a calcination of the powder at 623 K (550°C) reduced the pH shift, but it could not be eliminated completely. An explanation for this behaviour would be the incorporation of ammonia in the silica particles during their synthesis. The very slow release process may be attributed to a strong adsorption potential and/or to exceedingly small pore openings (of the same size as NH_3) in the particles, hindering the escape of the ammonia molecule from the particle core.

In a similar way nitrogen sorption measurements also indicated an ultramicroporous structure of the particles.[13,39] Nitrogen sorption isotherms were determined point by point by measuring the 'equilibrium' adsorbed mass of nitrogen at the respective adjusted relative pressures. However, it proved to be difficult to determine the true equilibrium values. At a chosen gas pressure the adsorbed amount reached an approximate plateau value within a few minutes; nevertheless, a very slow but continuous further uptake was noticed over more than two days. In addition, the desorption branch of the isotherm did not meet the adsorption branch at low relative pressures, indicating the inaccuracy of the determined data points. In consequence, the calculated BET surface areas were somewhat larger than the calculated geometrical surface area of the silica particles. However, a better correlation was noticed when the specific surface area was calculated from mercury porosimetry measurements[39] or in cases when the adsorption data were determined within a short time (less than 1 h for all data points in the BET region; relative pressure: $P/P_0 < 0{\cdot}6$). Likewise, sorption studies, which used different inert gases at room temperature, also indicated ultramicropores.[40] The adsorbed amounts and the kinetics of the adsorption process indicated that some gas molecules were allowed to penetrate the particles whereas others were excluded. For example, the adsorbed amount of helium or argon was roughly 10 to 100 times more than the amounts of krypton or xenon under the same conditions, suggesting a cut-off pore size of about 0·3 nm.

Another fact which can be an indication for the porous structure of the particles was the density of the powders. Densities determined with the helium or water pycnometer were $\leq 2{\cdot}0$ g cm^{-3} for all original silica samples. On calcination at $\geq$1073 K (800°C) it increased to the literature value of amorphous silica (2·2–2·25 g cm^{-3}). Since no crystalline phases developed during this calcination, the density change was obviously due to some rearrangement within the particles, which, on the other hand, was only possible when the original particles had a porous structure. The low density of the original Stöber silica particles was also observed by several other groups.[3,10,21,36] For example, van Helden *et al.*[36] reported densities of as low as 1·61 g cm^{-3} for some of their silica samples. The latter density would suggest a porosity of about 25–30 vol.%.

Last but not least, some of the silica samples displayed a particulate structure on TEM micrographs. An example is shown in Fig. 5. The size of the subunits was well below 10 nm, but it varied from sample to sample and quite often no structure was visible at all.

3.5 Precipitation reaction

In principle, the reaction of TEOS to form silica can be divided into two major steps: the hydrolysis and the condensation reaction. It is now the purpose of the following paragraphs to give some further details of this reaction; even so, the complete reaction is still far from a full understanding, since there are numerous reaction intermediates and possible reaction pathways to account for.

3.5.1 Reaction intermediates

In this study the trimethylsilation technique was used to determine the reaction intermediates. Low molecular weight silicate units of up to 20 Si units can be identified by gas chromatography in this way. Furthermore the overall particle growth reaction was stopped, since all reactive sites (hydroxyl groups) on the surface of existing nuclei were blocked by the trimethylsilyl groups.

Several reaction mixtures, according to Table 1, were studied in further detail by the trimethylsilation technique. Irrespective of differences in the overall reaction rates, the percentages among the low molecular weight units did not change very much with reaction time and no characteristic

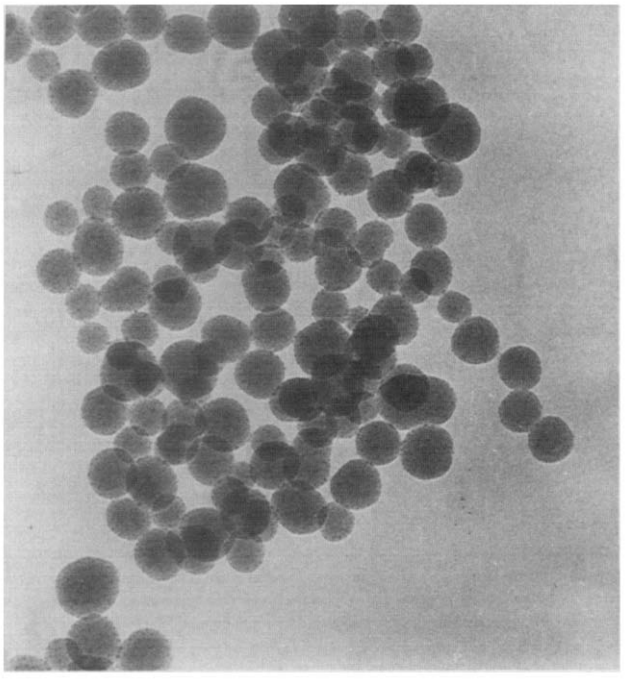

Fig. 5. Transmission electron micrographs of silica particles, demonstrating the nanometer-sized substructures. (Original magnification × 666 000.)

trend was noticed. Probably differences existed for the very first reaction period (<1 min), but it was difficult to take samples during this time and the scattering of the obtained data prohibited any further conclusions. In particular, 70–90% monomer, 10–25% dimer, <2% trimer silicic acid units, and hardly any higher oligomers (<1%) were observed. These findings were in accordance with results by Rothbaum & Rohde.[41] They observed 1–7% dimer and 0·1–1% trimer units on polymerization of monomeric silicic acid. The results proved that monomer and dimer silicate units were the major reaction intermediates under the chosen (basic) conditions. Moreover, the particle growth must proceed by addition of these units rather than by addition of higher oligomers.

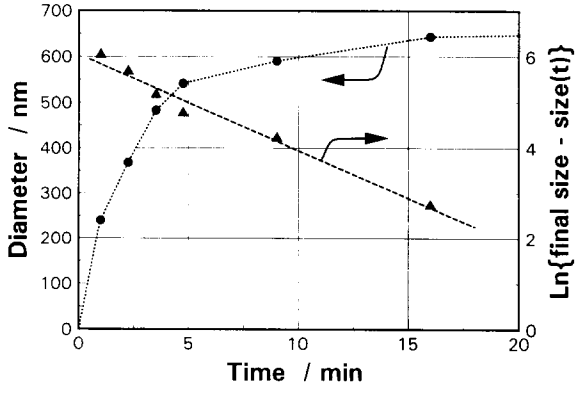

Fig. 6. Particle size (●, left y-axis) and the converted reaction yield (Δ, right y-axis), assuming a first order reaction, plotted as a function of time in a mixture of 3·0 mol dm^{-3} ammonia, 8·0 mol dm^{-3} water, and 0·2 mol dm^{-3} TEOS at 313 K (40°C). The data were determined from TEM micrographs after terminating the reaction by addition of trimethylchlorosilane.

3.5.2 Particle growth

The particle size was 'frozen' immediately after the addition of $(CH_3)_3SiCl$. The particle growth reaction could be followed by stopping the reaction after various times. The TEM micrographs of the latter samples indicated a monomodal particle size distribution for all reaction times and no smaller subunits or nuclei were observed. Figure 6 presents a plot of the particle size versus the reaction time for one sample. A first-order reaction was expected and the corresponding plot of the converted data (second y-axis in Fig. 6) resulted in a linear relation of the data points, thus verifying the previous assumption.

3.5.3 Reaction rate

As described in the previous paragraph, the reaction rate could be evaluated point by point after stopping the particle growth and determining the particle size from the corresponding TEM micrographs. This technique was very accurate and presented various other information, like particle uniformity or size distribution, but it was also very time consuming. Therefore a simple light-scattering technique (see experimental part) was employed to record the particle growth *in situ*. The light-scattering data had to be converted into the corresponding particle size or reaction yield, which was simplified by the fact that the scattering intensity was proportional to the particle mass over most of the observed range. A few typical curves are shown in Fig. 7. Depending on the reaction conditions the particle growth was completed within a few minutes or it took several hours.

A comparison with different reaction mechanisms—first- or second-order reaction, diffusion-controlled, monomolecular or polymolecular growth mechanisms[42]—demonstrated the best fit for the first-order reaction.[13] This observation was in agreement with the result of the trimethylsilation experiment, shown in Fig. 6, or most of the published data.[17,19,25,28] The calculated first-order reaction rates, observed in the different mixtures, are listed in Table 1. Table 2 presents the outcome of the corresponding factorial analysis. It follows from the latter results that all reaction parameters—temperature, ammonia and water concentration—had an obvious effect on the reaction rate. All linear parameters and combinations thereof demonstrated a highly significant influence by a probability of over 99%. Moreover, the quadratic effect of the temperature demonstrated its influence at a significance of >95% and all other parameters were negligible.

With increasing water and ammonia concentration or reaction temperature the reaction rate

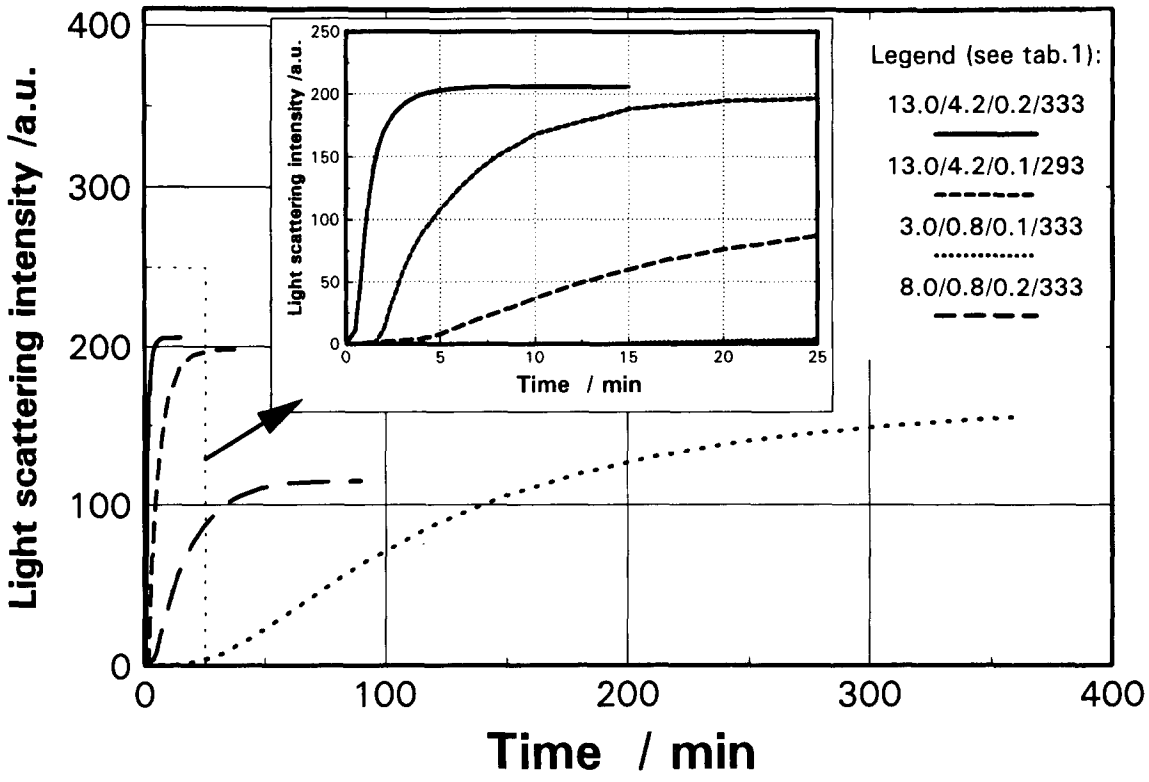

Fig. 7. Light-scattering intensity (reaction conversion) as a function of time. The legend refers to the reaction conditions as set out in Table 1. The numbers represent H_2O, NH_3, TEOS conc. and temperature. The inserted diagram shows the curves on an expanded time scale, demonstrating the large differences in the induction period.

always increased. The corresponding three-dimensional graph (Fig. 8) of the reaction rate versus water and ammonia concentration at the three temperatures clearly demonstrates this relationship.

Likewise the data were taken to determine the reaction orders relative to the water and ammonia concentration. The logarithm of the reaction rate was plotted versus the logarithm of the water or ammonia concentration respectively. Each set of three data points, which were obtained under otherwise equal conditions, were connected by a line and the average value of the slope of all of these curves corresponded to the reaction order of the viewed parameter. A reaction order of 0·97 and 1·18 was observed for the ammonia and the water concentration, respectively. The latter values agreed well with the data given by Harris *et al.*[19] ammonia: 0·9 and water: 1·5.

In a similar way the activation energy of the particle growth reaction was determined by plotting the logarithm of the reaction rate versus the

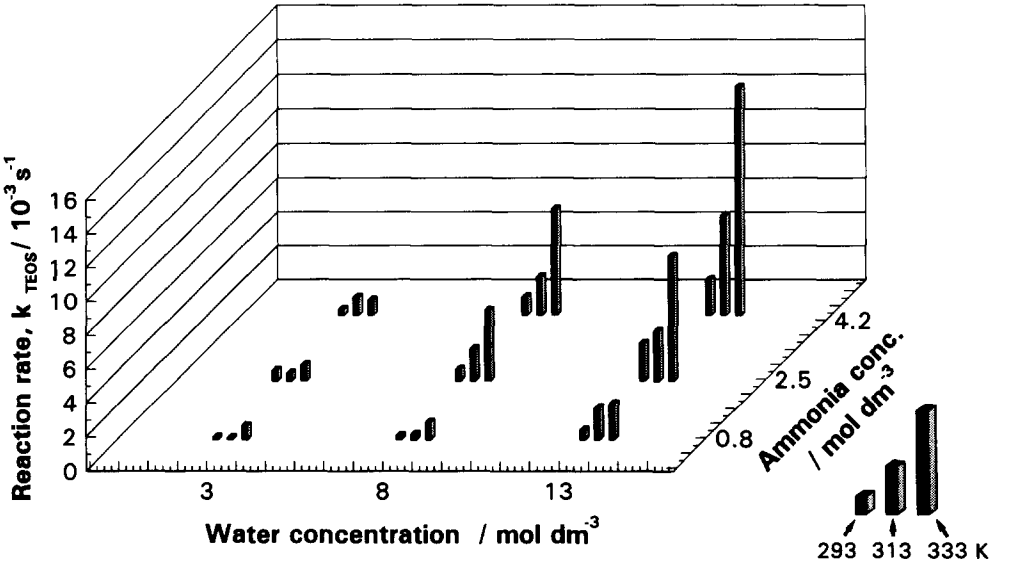

Fig. 8. Three-dimensional plot of the particle growth reaction rate, k_{TEOS}, versus the water and ammonia concentration of the reaction mixture at a constant TEOS concentration of 0·2 mol dm^{-3}. The left, middle and right bars of each data triplet indicate results at reaction temperatures of 293, 313, 333 K (20, 40, 60°C), respectively.

inverse of the reaction temperature (in K). The observed value of E_A = 27 kJ mol^{-1} (6·5 kcal mol^{-1}) fell within the range of various literature data[41,43–47] for the polymerization or precipitation reaction in silica systems.

The growth reaction rate can now be summarized as follows.

$$\mathrm{d[SiO_2\ particle]}/\mathrm{d}t = k_{\mathrm{TEOS}}\,[\mathrm{TEOS}]$$

$$= k' \exp\left\{\frac{-E_a}{RT}\right\} [\mathrm{H_2O}]^{1.18}\,[\mathrm{NH_3}]^{0.97}\,[\mathrm{TEOS}]$$

$$= 2{\cdot}36\ \mathrm{s^{-1}(mol\ dm^{-3})^{-2.15}} \exp\left\{\frac{-3256\ \mathrm{K}}{T}\right\} \times [\mathrm{H_2O}]^{1.18}\,[\mathrm{NH_3}]^{0.97}\,[\mathrm{TEOS}] \quad (1)$$

The constant, k', was calculated from the reaction rates given in Table 1 according to eqn (1). Its average value was: k' = 2·36 s^{-1}(mol dm^{-3})$^{-2.15}$. Moreover, reaction rates published in the literature[17,19,25,28] were compared with the corresponding values calculated from eqn (1), shown in Fig. 9. Although the overall agreement was adequate, a small systematic difference towards higher values was seen in the data of van Blaaderen *et al.*,[28] whereas the reaction rates published by Bogush & Zukoski[25] always exhibited slightly lower values than calculated. On the other hand, within each set of literature data the linear relation between experimental and calculated values was excellent, as indicated by the correlation coefficients of r^2 = 0·997 and 0·994, respectively. Nonetheless, the general agreement was very remarkable, since the literature data were obtained by completely different techniques and in addition, the reaction rates used for the evaluation of eqn (1) and the values of the constants, k' and E_a were determined by the very simple light-scattering device described in the experimental part.

3.5.4 Induction period

The induction period was evaluated from the light-scattering curves as well. It was defined as the time interval until the scattering intensity deviated from its starting value (derived by extrapola-

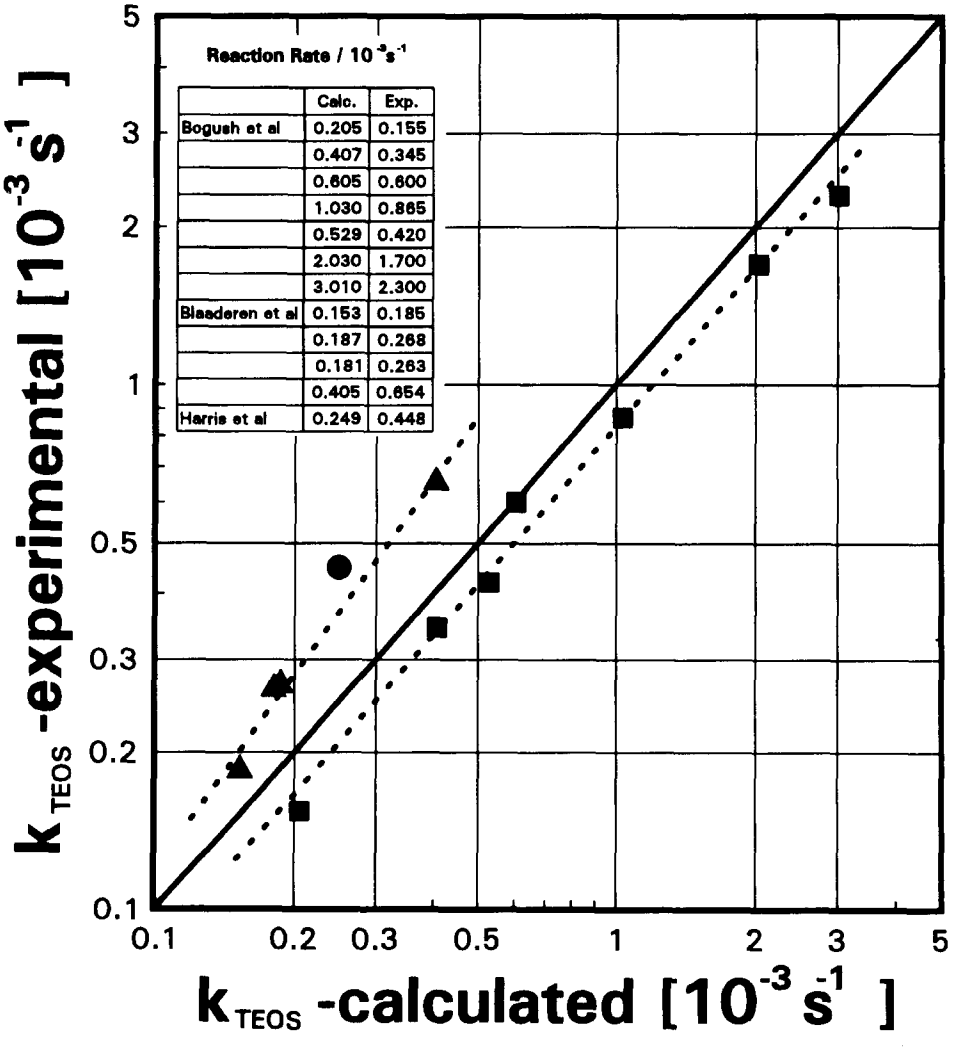

Fig. 9. Plot of SiO_2 particle growth or TEOS hydrolysis rates, as determined experimentally by Bogush & Zukoski,[26] van Blaaderen *et al.*,[28] Harris *et al.*[19] or Matsoukas & Gulari[17,18] versus the corresponding calculated values according to eqn (1). Dotted lines represent the linear regression of the data of Bogush & Zukoski[26] and van Blaaderen *et al.*[28] having correlation coefficients r^2 = 0·994 and 0·997, respectively.

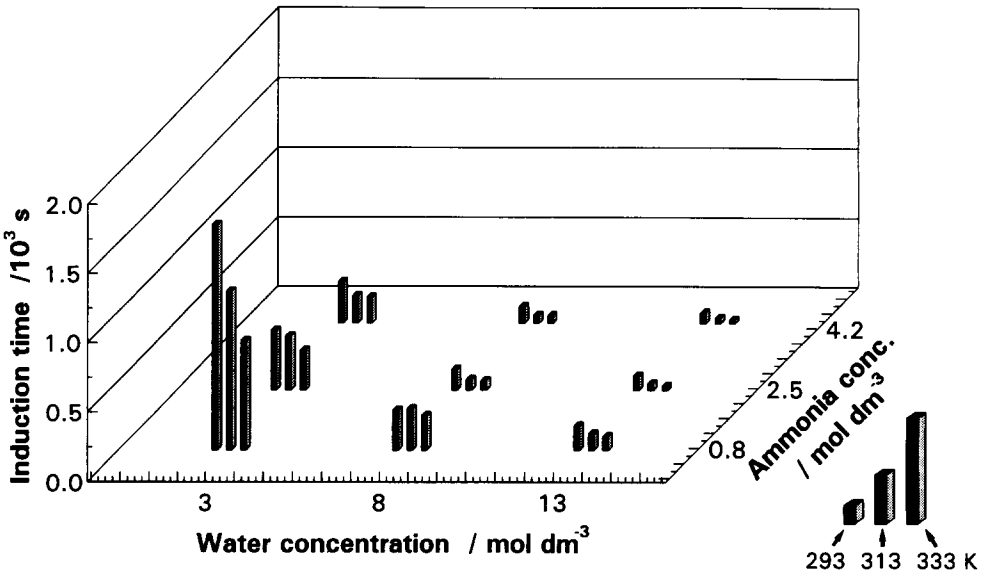

Fig. 10. Three-dimensional plot of the induction time, determined by extrapolation from the light-scattering curves, versus the water and ammonia concentration of the reaction mixture at a constant TEOS concentration of 0·2 mol dm^{-3}. The left, middle and right bars of each data triplet indicate results at reaction temperatures of 293, 313, 333 K (20, 40, 60°C), respectively.

tion). This time varied over a wide range from 27 s up to about 30 min. Influences on the induction period were evaluated by a statistical analysis, as shown in Table 2. The linear water and ammonia effect and their combination were of highest significance as shown by their very high variance ratios, but clearly many other parameters or combinations thereof were also of importance (at probabilities of >99% or >95%, see Table 2). Due to the various quadratic and combined effects, being of a certain statistical importance, the overall conclusions were not as clear cut as the analogous results for the reaction rate. The three-dimensional plot (Fig. 10) of the induction period versus the water and ammonia-concentration or temperature graphically illustrated the main results. The induction period decreased with increasing water and ammonia content or temperature. A comparison of Figs 8 and 10 now clearly demonstrated the inverse behaviour of induction period and reaction rate. This relation was understandable, since there was no indication that these parameters would be controlled by completely different reaction mechanisms. It was obvious that a fast overall reaction would most probably shorten the 'nucleation' or 'induction' period too.

3.5.5 Comparison with models

Many papers have been published concerning the hydrolysis and condensation reaction in the silicate system. The majority of them have been dealing with the reaction under acidic conditions, when silica polymers or gel structures are formed. On the other hand, the base-catalysed reaction, especially in the presence of ammonia, has been studied only recently in more detail.[17–28] In addition, the Stöber process, as the most prominent example of the base-catalysed silica reaction, is an ideal example to study the formation of monodispersed particles. At present there are two major models to explain the particle formation process in the Stöber silica system. First, there is the monomer addition growth model,[18] in analogy to a 'LaMer' precipitation diagram,[48] which describes the nucleation by exceeding the supersaturation limit and the growth by condensation of monomeric silicic acid on the surface of the existing particles (nuclei). It is mainly a chemical type of explanation, focusing on the hydrolysis and condensation rate and the solubility of silicic acid. Second, nucleation and growth of particles is modelled by a controlled aggregation mechanism of sub-particles, a few nanometer in size.[26] Colloidal stability, nuclei size, surface charge and diffusion and aggregation characteristics are the important parameters in this model. The two models seem to be nearly incompatible in several aspects and it should be easy to distinguish between them. However, there were a number of observations, shown here or in other publications, which clearly support either the first or the second model.

3.5.5.1 Monomer addition growth model. In the following section, experimental results of the present study will be discussed in relation to the previously mentioned models and compared with literature data. For example, the particle growth could be best described by a first-order reaction with respect to the TEOS concentration. Even so, there are several publications favouring a second-, third-, or fourth-order reaction for the polymerization of silicic acid (for further details, see Iler[49] or Rothbaum & Rohde[41]). Most of

the recent publications,[17–19,25,28] concerning the 'Stöber' silica precipitation, agreed with the results shown here and describe a first-order hydrolysis of TEOS as the rate-limiting process in the silica particle precipitation. The second reaction step, the condensation reaction, was found to be faster by at least a factor of three.[25,26,28]

Moreover, the appearance of an induction period would also favour a LaMer-type mechanism, since it will take a certain time for the hydrolysis of TEOS to exceed the equilibrium or the critical nucleation concentration of silicic acid in the solution followed by precipitation of silica. Yet the latter hypothesis is somehow incompatible with the observations of an induction period in seeded growth experiments by van Blaaderen *et al.*[28] or Philipse.[5] In these experiments silica seeds were prepared and grown in the same solution, and therefore the silicic acid concentration should be already at or above its equilibrium value, and consequently, as soon as some further TEOS was hydrolysed, the condensation reaction or the particle growth reaction should take place. Nonetheless, an induction period was again observed. This discrepancy between expected and observed behaviour can be explained. Fleming[46] studied the dissolution and precipitation rate of silica in dependence on the free silicic acid concentration near its solubility equilibrium. His results indicated that the precipitation rate decreased linearly with decreasing silicic acid concentration. However, the point where the deposition rate dropped to nearly zero was observed at a silica concentration which was about twice its equilibrium value. Thereafter a very slow drift towards the final equilibrium was noticed. Fleming explained this drift by a different solubility of fresh and aged silica. It follows for the case of seeded growth experiments that such a drift will occur in a similar way after the first step, the preparation of the seed particles. Obviously it will take a certain amount of TEOS to be hydrolysed, before the concentration of free silicic acid reaches the 'first equilibrium' again and the precipitation or the particle growth starts after exceeding this value.

3.5.5.2 Aggregation growth model. On the other hand, there were several results which referred to an agglomerated structure of the particles. The most prominent evidence was the structures seen in some of the TEM micrographs (see Fig. 5), but also the measured densities (up to 30% lower than the theoretical value), the incorporation of ammonia in the particles, the high specific surface area, the slow kinetics in nitrogen adsorption measurements, or the observed cut-off size in adsorption experiments using different inert gases.[40] All of these were clear indications of an ultramicroporous structure of the silica powders. The question remained, how such a porous structure developed during the synthesis.

The simplest explanation was given by an aggregation growth model, described for example by Bogush & Zukoski[26] or Philipse.[5] Small silica nuclei of several nanometer in size form continuously during the hydrolysis and condensation reaction of TEOS. These nuclei are colloidally unstable and they will coagulate and form larger units. These are stable above a critical size and their further growth is accomplished by addition of subsequent primary nuclei to the existing 'particle' surface of the agglomerates. The number and size of these units will be determined not only by the reaction kinetics, but also by different parameters effecting the dispersion stability, like the ionic strength of the solution, temperature, charges on the particle surface, pH, solvent properties (viscosity, dielectric constant, etc) and so on.

Bogush & Zukoski[25,26] could explain several of their observations with this model. For example, the final particle size increased from 343 nm to 710 nm Ø, when the precipitation mixture contained 10^{-2} mol dm^{-3} NaCl; even so, the reaction rate remained nearly constant at $k_{TEOS} = 1 \times 10^{-3}$ s^{-1}. This observation was explained by the lower colloidal stability in the system containing the higher NaCl concentration (higher ionic strength). Due to this, a smaller number of aggregate units were formed at the beginning and consequently particles grew larger in size.

Further evidence for such a picture of particles made by aggregation of primary nuclei was given by results of van Helden *et al.*[36] They repeatedly observed a second peak in SAXS measurements on Stöber silica particles. The authors questioned whether this result was real or an artefact. The position of the peak was always noticed around a structural size of 1 nm. The latter value for the critical size of silica nuclei was in very good conformity with calculations by Makrides *et al.*[45] Depending on the chosen values for the interfacial energy (silica/solution), the silica concentrations, and the temperature, the authors calculated a critical size of about 1 to 2 nm.

The formation of these primary nanometer-sized subunits as an intermediate step in the growth reaction could also account for the observed induction period. The condensation reaction can proceed parallel to the hydrolysis reaction from the very first beginning and still it will take a certain time (induction time) to produce the primary subunits, which then may agglomerate or adhere to the surface of seed particles.

On the contrary, results of the trimethylsilation experiments presented here, stayed in clear contrast to an aggregation growth model. Mostly monomer, some dimer and only insignificant amounts of higher oligomeric silicate units were detected throughout the whole precipitation reaction. This opposed the production of nanometer-sized nuclei as requested by the aggregation growth model, since at least a certain amount of higher oligo-meric units should be detected, representing the intermediate steps towards these primary nuclei. The trimethylsilation data obviously favoured the monomer addition growth model. However, it has to be noticed that these results were obtained at reaction times when the first formation of particles was already passed (after the induction period).

3.5.5.3 Eden growth model. A different explanation for the development of a porous structure is given by Keefer and coworker.[50,51] The nucleation and random growth of clusters from partially hydrolysed monomers was simulated. The Eden growth model, used in that study, resulted in more or less porous structures. The fractal structures depended strongly on the assumed degree of hydrolysis of monomeric silica units. Fully hydrolysed monomers resulted in relative dense particles, whereas the structure became more open with only partly hydrolysed silicate building units.

4 Conclusion

The Stöber silica preparation process was studied over a wide range of experimental conditions (TEOS, NH_3, H_2O concentration and temperature). Particle properties—size, distribution, shape and structure—as well as reaction kinetics—growth rate and induction period—were evaluated by a statistical analysis. The mean particle size was influenced by all experimental parameters, whereas the effect on size distribution and shape of the particles was much less pronounced. All samples were relative monodisperse, but a trend towards a narrower distribution or a more spherical shape was observed at higher water concentrations. The particles showed an ultramicroporous internal structure, as revealed by TEM micrographs or adsorption measurements.

Analysis of the reaction kinetics revealed that only monomeric and some dimeric silicic acid was detected as intermediate silicate units in the solution. The particle growth could best be described by a first-order process relative to the TEOS concentration. The reaction orders relative to the water and ammonia concentration were 1·18 and 0·97, respectively, and an activation energy of 27 kJ mol^{-1} (6·5 kcal mol^{-1}) was determined for the reaction, resulting in the following equation:

$$d[SiO_2\ \text{particle}]/dt = 2{\cdot}36\ s^{-1}(\text{mol dm}^{-3})^{-2{\cdot}15} \times \exp\left\{\frac{-3256\ \text{K}}{T}\right\} [H_2O]^{1{\cdot}18}\ [NH_3]^{0{\cdot}97}\ [\text{TEOS}]$$

The induction period was inversely related to the reaction rate and clearly influenced by the same parameters.

The results were compared with particle formation models and the following mechanism appeared to be most realistic. Nanometer-sized subunits were formed during the very first reaction stage, followed by a controlled aggregation to larger units. The colloidal stability and aggregation rate of the primary nuclei determined the number and size of the particles. However, the growth mechanism changed at a later stage in the reaction and thereafter particles grew solely by condensation of monomeric and dimeric silicate units at the particle surface. The point at which the reaction mechanism changed, depended very much on the overall reaction conditions. Similar conclusions were drawn by van Blaaderen *et al.*[28] and Harris *et al.*[19] They also concluded that the particle formation started with the aggregation of siloxane substructures and proceeded further through a surface reaction-limited condensation of hydrolysed monomers or small oligomers. Harris *et al.*[19] assumed the change in mechanism at a particle size of about 100 nm in their experiments.

Acknowledgements

The author would like to thank Professor K. K. Unger for an introduction to this fascinating field of science and is grateful for his guidance and support throughout this work. Finally the Deutsche Forschungsgemeinschaft is thanked for their financial support through Grant Number Un 26/25-1.

References

1. Kolbe, G., Das komplexchemische Verhalten der Kieselsäure. Dissertation, Friedrich-Schiller Universität Jena, 1956.
2. Stöber, W., Fink, A. & Bohn, E., Controlled growth of monodisperse silica spheres in the micron size range. *J. Colloid Interface Sci.*, **26** (1968) 62–9.
3. Van Helden, A. K. & Vrij, A., Contrast variation in light scattering: silica spheres dispersed in apolar solvent mixtures. *J. Colloid Interface Sci.*, **76** (1980) 418–33.
4. Philipse, A. P. & Vrij, A., Polydispersity probed by light scattering of secondary particles in controlled growth experiments of silica spheres. *J. Chem. Phys.*, **87** (1987) 5634–43.
5. Philipse, A. P., Quantitative aspects of the growth of

(charged) silica spheres. *Colloid Polym. Sci.*, **266** (1988) 1174–80.
6. Philipse, A. P. & Vrij, A., Preparation and properties of nonaqueous model dispersions of chemically modified, charged silica spheres. *J. Colloid Interface Sci.*, **128** (1989) 121–36.
7. van der Werff, J. C. & de Kruif, C. G., Blom, C. & Mellema, J., Linear viscoelastic behavior of dense hard-sphere dispersions. *Phys. Rev. A*, **39** (1989) 795–807.
8. van der Werff, J. C. & de Kruif, C. G., Hard-sphere colloidal dispersions: the scaling of rheological properties with particle size, volume fraction, and shear rate. *J. Rheol.*, **33** (1989) 421–54.
9. Jones, D. A. R., Leary, B. & Boger, D. V., The rheology of a concentrated colloidal suspension of hard spheres. *J. Colloid Interface Sci.*, **147** (1991) 479–95.
10. Chen, M. & Russel, W. B., Characteristics of flocculated silica dispersions. *J. Colloid Interface Sci.*, **141** (1991) 564–77.
11. Ackerson, B. J., Shear induced order and shear processing of model hard sphere suspensions. *J. Rheol.*, **34** (1990) 553–90.
12. Emmett, S., Lubetkin, S. D. & Vincent, B., The growth of ordered sediments of monodispersed hydrophobic silica particles. *Colloids Surfaces*, **42** (1989) 139–53.
13. Giesche, H., Modellporenkörper aus monodispersen sphärischen SiO_2-Partikeln: Herstellung, Charakterisierung und Sinterverhalten. Dissertation, Universität Mainz, 1987.
14. Sacks, M. D. & Tseng, T.-Y., Preparation of SiO_2 glass from model powder compacts: I, formation and characterization of powders, suspensions, and green compacts. *J. Am. Ceram. Soc.*, **67** (1984) 526–32.
15. Sacks, M. D. & Tseng, T.-Y., Preparation of SiO_2 glass from model powder compacts: II, sintering. *J. Am. Ceram. Soc.*, **67** (1984) 532–7.
16. Giesche, H. & Unger, K. K., Sintering of monodispersed silica. In *Proceedings of Ceramic Powder Processing Science, 2nd International Conference*, Berchtesgaden, 1988, ed. H. Hausner, G. L. Messing & S. Hirano. Deutsche Keramische Gesellschaft, Köln, 1989, pp. 755–64.
17. Matsoukas, T. & Gulari, E., Dynamics of growth of silica particles from ammonia-catalyzed hydrolysis of tetraethyl-orthosilicate. *J. Colloid Interface Sci.*, **124** (1988) 252–61.
18. Matsoukas, T. & Gulari, E., Monomer-addition growth with a slow initiation step: a growth model for silica particles from alkoxides. *J. Colloid Interface Sci.*, **132** (1989) 13–21.
19. Harris, M. T., Basaran, O. A. & Byers, C. H., The precipitation dynamics of silica particles. In *Ceramic Transactions*, Vol. 12, *Ceramic Powder Science III*, ed. G. L. Messing, S.-I. Hirano & H. Hausner. The American Ceramic Society Inc., Westerville, OH, 1990, pp. 119–27.
20. Bogush, G. H., Dickstein, G. L., Lee, P., Zukoski, K. C. & Zukoski IV, C. F., Studies of the hydrolysis and polymerization of silicon alkoxides in basic alcohol solutions. In *Mater. Res. Soc. Symp. Proc.*, Vol. 121, *Better Ceramics Through Chemistry III*, ed. Jeffrey C. Brinker, D. E. Clark & D. R. Ulrich. Materials Research Society, Pittsburgh, PA, 1988, pp. 57–65.
21. Bogush, G. H., Tracy, M. A. & Zukoski IV, C. F., Preparation of monodisperse silica particles: control of size and mass fraction. *J. Non-Cryst. Solids*, **104** (1988) 95–106.
22. Bogush, G. H., Brinker, C. J., Majors, P. D. & Smith, D. M., Evolution of surface area during the controlled growth of silica spheres. In *Materials Research Society Symposium Proceedings*, Vol. 180, *Better Ceramics Through Chemistry IV*, ed. B. J. J. Zelinski, J. C. Brinker, D. E. Clark & D. R. Ulrich. Materials Research Society, Pittsburgh, PA, 1990, pp. 491–4.
23. Look, J.-L., Bogush, G. H. & Zukoski, C. F., Colloidal interactions during the precipitation of uniform submicrometre particles. *Faraday Discuss. Chem. Soc.*, **90** (1990) 345–57.
24. Kim, S. & Zukoski, C. F., A model of growth by heterocoagulation in seeded colloidal dispersions. *J. Colloid Interface Sci.*, **139** (1990) 198–212.
25. Bogush, G. H. & Zukoski, IV, C. F., Studies of the kinetics of the precipitation of uniform silica particles through the hydrolysis and condensation of silicon alkoxides. *J. Colloid Interface Sci.*, **142** (1991) 1–18.
26. Bogush, G. H. & Zukoski IV, C. F., Uniform silica particle precipitation: an aggregative growth model. *J. Colloid Interface Sci.*, **142** (1991) 19–34.
27. den Ouden, C. J. J. & Thompson, R. W., Analysis of the formation of monodisperse populations by homogeneous nucleation. *J. Colloid Interface Sci.*, **143** (1991) 77–84.
28. van Blaaderen, A., van Geest, J. & Vrij, A., Monodisperse colloidal silica spheres from tetraalkoxysilanes: particle formation and growth mechanism. *J. Colloid Interface Sci.*, **154** (1992) 481–501.
29. Calhoun, H. P. & Masson, C. R., In *Reviews on Silicon, Germanium, Tin and Lead Compounds*, ed. M. Gielen. Freund Publishing House, Tel-Aviv, 1981, p. 153.
30. Garzo, G., Hoebbel, D., Ecsery, Z. J. & Ujszaszi, K., Gas chromatography of trimethylsilylated silicate anions—separation with glass capillary columns and new aspects in derivatization. *J. Chromatography*, **167** (1978) 321–36.
31. Bechtold, M. F., Vest, R. D. & Plambeck Jr, L., Silicic acid from tetraethyl silicate hydrolysis. Polymerization and properties. *J. Am. Chem. Soc.*, **90** (1968) 4590–8.
32. Schubert, P., Der Einfluss der Silikatquelle auf die Synthese von ZSM-5—neue Wege zur Synthese und Charakterisierung. Dissertation, Universität Mainz, 1985.
33. Straube, B., Kritische Untersuchung und Standardisierung physikalisch-chemischer Messmethoden zur Ermittlung der spezifischen Oberfläche und Porenverteilung von Adsorbentien. Dissertation, Universität Mainz, 1985.
34. Davies, O. L., *The Design and Analysis of Industrial Experiments*. Oliver and Boyd, London, 1967.
35. Giesche, H., Untersuchung über die Herstellung und Agglomeration von monodispersen Kieselsäuresolen. Diplomarbeit, Mainz, 1983.
36. van Helden, A. K., Jansen, J. W. & Vrij, A., Preparation and characterization of spherical monodisperse silica dispersions in nonaqueous solvents. *J. Colloid Interface Sci.*, **81** (1981) 354–68.
37. Tan, C. G., Bowen, B. D. & Epstein, N., Production of monodisperse colloidal silica spheres: effect of temperature. *J. Colloid Interface Sci.*, **119** (1987) 290–3.
38. Unger, K. K., Giesche, H. & Kinkel, J. N., Kugelförmige SiO_2-Partikel. DE Patents 3534143 A1, 25 September 1985; 3616133 Al, 14 May 1986; US Patents 4911903, 27 March 1990, 4775520, 4 October 1988.
39. Giesche, H., Unger, K. K., Müller, U. & Esser, U., Hysteresis in nitrogen sorption and mercury porosimetry on mesoporous model adsorbents made of aggregated monodisperse silica spheres. *Colloids Surfaces*, **37** (1989) 93–113.
40. Reichert, H., Adsorptionsuntersuchungen an SiO_2-Agglomeraten. Diplomarbeit, Universität Mainz, 1988.
41. Rothbaum, H. P. & Rohde, A. G., Kinetics of silica polymerization and deposition from dilute solutions between 5 and 180°C. *J. Colloid Interface Sci.*, **71** (1979) 533–59.
42. Nielsen, A. E., *Kinetics of Precipitation*. Pergamon Press, New York, 1964.
43. Bohlmann, E. G., Mesmer, R. E. & Berlinski, P., Kinetics of silica deposition from simulated geothermal brines. *Soc. Petroleum Eng. J.*, (1980) 239–48.
44. Weres, O., Yee, A. & Tsao, L., Kinetics of silica polymerization. *J. Colloid Interface Sci.*, **84** (1981) 379–402.
45. Makrides, A. C., Turner, M. & Slaughter, J., Condensation of silica from supersaturated silicic acid solutions. *J Colloid Interface Sci.*, **73** (1980) 345–67.

46. Fleming, B. A., Kinetics of reaction between silicic acid and amorphous silica surfaces in NaCl solutions. *J. Colloid Interface Sci.*, **110** (1986) 40–64.
47. Brady, A. P., Brown, A. G. & Huff, H., The polymerization of aqueous potassium silicate solutions. *J. Colloid Interface Sci.*, **8** (1953) 252–76.
48. LaMer, V. K. & Dinegar, R. H., Theory, production and mechanism of formation of monodispersed hydrosols. *J. Am. Chem. Soc.*, **72** (1950) 4847–54.
49. Iler, R. K., *The Chemistry of Silica*. Wiley, New York, 1979.
50. Keefer, K. D., Growth and structure of fractally rough silica colloids. In *Better Ceramics through Chemistry II, Mat. Res. Soc. Symp. Proc.*, Vol. 73, ed. J. C. Brinker, D. E. Clark & D. R. Ulrich. Materials Research Society, Pittsburgh, PA, 1986, pp. 295–304.
51. Keefer, K. D. & Schaefer, D. W., Growth of fractally rough colloids. *Phys. Rev. Lett.*, **56** (1986) 2376–9.